

Construction of an invertible mapping to boundary conforming coordinates for arbitrarily shaped toroidal domains.

Robert Babin^{1,2}, Florian Hindenlang¹, Omar Maj¹ and Robert Köberl^{1,2}

¹ Numerical Methods in Plasma Physics, Max Planck Institute for Plasma Physics, Garching, Germany

² School of Computation, Information and Technology, Technical University of Munich, Munich, Germany

E-mail: robert.babin@ipp.mpg.de

Abstract. Boundary conforming coordinates are commonly used in plasma physics to describe the geometry of toroidal domains, for example, in three-dimensional magnetohydrodynamic equilibrium solvers. The magnetohydrodynamic equilibrium configuration can be approximated with an inverse map, defining nested surfaces of constant magnetic flux. For equilibrium solvers that solve for this inverse map iteratively, the initial guess for the inverse map must be well defined and invertible. Even if magnetic islands are to be included in the representation, boundary conforming coordinates can still be useful, for example to parametrize the interface surfaces in multi-region, relaxed magnetohydrodynamics. Given a fixed boundary shape, finding a valid boundary conforming mapping can be challenging, especially for the non-convex boundaries from recent developments in stellarator optimization. In this work, we propose a new algorithm to construct such a mapping, by solving two Dirichlet-Laplace problems via a boundary integral method. We can prove that the generated harmonic map is always smooth and has a smooth inverse. Furthermore, we can find a discrete approximation of the mapping that preserves this property.

Keywords: boundary conforming coordinates, diffeomorphism, harmonic map, MHD, equilibrium

Submitted to: *Plasma Phys. Control. Fusion*

1. Introduction

In plasma physics for magnetic confinement fusion, the geometry of the plasma is often described by a toroidal domain, diffeomorphic to the solid torus. That is, there exists a differentiable and invertible mapping from the toroidal domain to the solid torus, with its inverse being differentiable as well. Besides cylindrical coordinates, other descriptions of the toroidal domain, like the Frenet-Serret frame or flux-aligned coordinates, are used. The latter are a type of boundary conforming coordinates, where one coordinate is radius-like and increases from the magnetic axis to the boundary of the domain, and the other two coordinates are angle-like and periodic with period 2π . In particular, for flux-aligned coordinates, the radial coordinate is constant on a family of nested toroidal surfaces on which the magnetic field is tangent, referred to as flux surfaces, and the angle-like coordinates parameterize these flux surfaces. Such coordinates are especially suited for spectral methods, e.g. employing Fourier-polynomial decomposition. State-of-the-art 3D magnetohydrodynamic (MHD) equilibrium solvers like VMEC [1] or GVEC [2] describe the magnetic field and flux surface geometry (in absence of magnetic islands) using an inverse coordinate representation, i.e. by describing the flux surface positions in real space (e.g. in Cartesian or cylindrical coordinates) as functions of the flux-aligned coordinates. Such codes find the equilibrium solution by iteratively changing the coordinate map in order to minimize energy. Therefore it is crucial that the initial mapping from flux-aligned coordinates to real space is well defined.

Recent developments in stellarator optimization using near-axis expansion [3–5] have resulted in strongly shaped plasma configurations. It is now of interest to explore configurations with similarly shaped plasma boundaries using higher-fidelity 3D MHD equilibrium solvers. However, initialization of equilibrium codes can be challenging with such boundaries, as conventional radial blending techniques (see Appendix A) between the plasma boundary and a specified initial magnetic axis fail. That is, they lead to overlapping flux surfaces and, thus, an invalid coordinate mapping. In addition, the position of the magnetic axis is a result of the equilibrium calculation and, as such, should not be needed for the initialization. There are algorithms to find an initial magnetic axis [6], but there are configurations where radial blending fails with any chosen axis. From a mathematical point of view, we are interested in finding boundary conforming coordinates for arbitrarily shaped toroidal domains.

As we only consider toroidal domains, we can further reduce the problem by one dimension and find two-dimensional boundary conforming coordinates for each cross-section of the toroidal domain. The domain is then composed of cross-sections that are parametrized by the toroidal angle. Finding boundary conforming coordinates for each cross-section is equivalent to finding a diffeomorphism from a two-dimensional, simply connected domain to the unit disk.

Recently a method was proposed to find a mapping from the solid torus to the considered domain using a variational principle which minimizes the squared Jacobian determinant of the domain with a penalty on the curvature of radial coordinate lines [7].

A similar problem is found in the context of boundary-fitted mesh generation, where a valid and smooth mesh needs to be generated in a domain that is only defined by its boundary. The boundary can be curved and also non-convex. A successful approach is the so-called elliptic mesh generator [8], which solves elliptic PDEs in order to generate the mesh. In particular, a well-known tool for structured grids is the solution of the Winslow equations, which results in so-called Laplace or Harmonic grids, first introduced by Winslow [9], and studied extensively since then, for example in [8, 10]. A variational formulation for the Winslow equations exists [11] and has been applied to unstructured high-order mesh generation [12]. The Winslow equations consist of two Laplace equations defined on the physical domain, and solving for the logical coordinates in order to find the mapping to the logical domain. Often, the Winslow equations are transformed to logical space, resulting in a nonlinear PDE for the mapping, and therefore, must be solved iteratively.

A simple solution that is guaranteed to exist for such a problem is a conformal map, for which there are also construction methods available. The conformal map is angle preserving and orthogonal, which is a strong constraint on the mapping and is often ill-suited for discretization, as can be seen for a simple domain bounded by an ellipse, discussed in section 4.2. In contrast, the elliptic domain can also be expressed by a linear transformation of the unit disk, discussed in section 2.2, which is not a conformal map, but easily discretized. Both the linear map and the conformal map are special cases of so called harmonic maps. In the case of planar domains, a harmonic mapping is defined by two coordinate functions that are harmonic [13]. That is, they are twice differentiable functions that satisfy Laplace's equation in the whole domain.

Inspired by these works, we propose a new algorithm to find boundary conforming coordinates for arbitrarily shaped toroidal domains. We will first construct a harmonic mapping from each poloidal cross-section of the domain to the unit disk. Note this is the inverse of the desired mapping. The harmonic mapping is constructed as the solution of two Laplace's equations with Dirichlet boundary conditions. In order to avoid having to discretize the domain with a mesh, we use a boundary integral method [14]. We can prove that the generated mapping is a diffeomorphism on the interior and thus invertible to obtain the desired mapping from the unit disk to the cross-section of the domain.

The paper is structured as follows. In section 2 we present the new method to construct the mapping from the 2D domain to the unit disk. In section 3, we prove the existence and regularity of the mapping, as well as that it is a diffeomorphism on the interior. In section 4 we present numerical results and finally present a discussion in section 5.

2. Proposed Method

The goal of this method is to construct boundary conforming coordinates in a domain defined by a given boundary curve, which is assumed to be a Jordan curve Γ , i.e. a planar simple closed curve. The domain $\Omega \subset \mathbb{R}^2$, delimited by the curve $\Gamma = \partial\Omega$, is

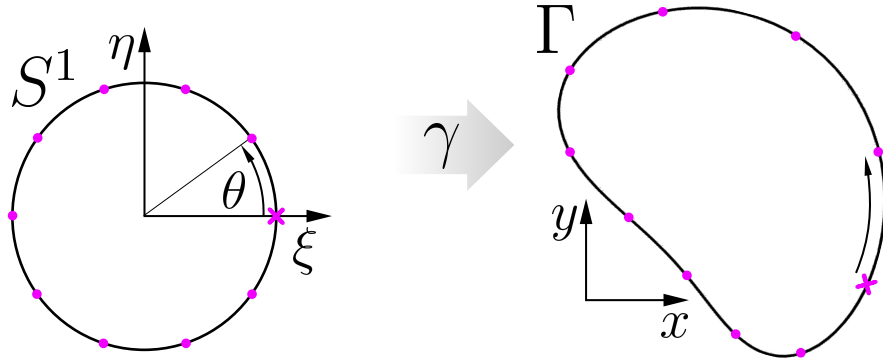


Figure 1. Sketch of the unit circle S^1 , a Jordan curve $\Gamma \subset \mathbb{R}^2$ and one possible parametrization $\gamma : S^1 \rightarrow \mathbb{R}^2$ with $\gamma(S^1) = \Gamma$. Equidistant points of θ are purple, with the point corresponding to $\theta = 0$ marked with a cross.

thereby an open, simply connected set. The Jordan curve Γ can be represented as the image of a function of an angle $\theta \in [0, 2\pi)$, which is in practice given as a (truncated) Fourier series or spline function. Because of the periodicity of the angle θ , it is convenient to view this function as a map defined on the unit circle $S^1 = \{e^{i\theta} : \theta \in [0, 2\pi)\}$, leading to the curve parametrization $\gamma : S^1 \rightarrow \mathbb{R}^2$, which is shown in figure 1. Furthermore, we require that γ is of class C^2 (twice continuously differentiable), and injective, so that γ is invertible on its image $\gamma(S^1) = \Gamma$.

The goal of the following construction is then to find a map $f : \bar{D} \rightarrow \bar{\Omega}$ from the unit disk $\bar{D} = \{z \in \mathbb{C} : |z| \leq 1\}$ to $\bar{\Omega}$, as depicted in figure 2. In order for f to define valid coordinates, it must be a diffeomorphism, i.e. f must be invertible and both f and f^{-1} must be continuously differentiable. We will construct f by inverting a harmonic map $g : \bar{\Omega} \rightarrow \bar{D}$, which is defined as the solution of two Laplace's equations with Dirichlet boundary conditions. Solutions of the Laplace's equation on such smooth

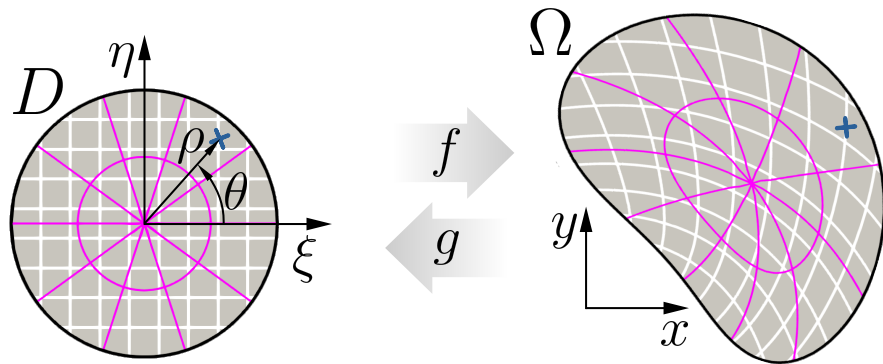


Figure 2. Sketch of the mapping between the unit disk D and a domain $\Omega \subset \mathbb{R}^2$. Lines of constant ρ, θ are purple, lines of constant ξ, η are white and the boundary is black. A blue cross marks an exemplary point in both domains, $\xi_\ell + i\eta_\ell = \rho_\ell \exp(i\theta_\ell) \leftrightarrow (x_\ell, y_\ell)$.

domains need to be twice continuously differentiable on the interior and continuous up to the boundary, i.e. of class $C(\overline{\Omega}) \cap C^2(\Omega)$. As seen from the comparison of figure 1 and figure 2, we additionally require that the angular parametrization of f , given by $z = \rho e^{i\theta}$, agrees at the boundary with the given boundary parametrization γ , i.e. $f(e^{i\theta}) = \gamma(e^{i\theta})$ for $\theta \in [0, 2\pi)$. For a given boundary shape, the following construction does not require any free parameters besides the parametrization of the boundary curve.

2.1. Construction of the harmonic map

Let $\Omega \subset \mathbb{R}^2$ be a simply connected domain bounded by a Jordan curve $\Gamma = \partial\Omega$ with C^2 parametrization $\gamma : S^1 \rightarrow \mathbb{R}^2$, γ being invertible on its image $\gamma(S^1) = \Gamma$. We construct the harmonic map

$$g : \overline{\Omega} \rightarrow \overline{D}, \quad (x, y) \mapsto \xi(x, y) + i\eta(x, y), \quad (1)$$

by imposing that $\xi, \eta \in C(\overline{\Omega}) \cap C^2(\Omega)$ are solutions to the Dirichlet-Laplace problems

$$\Delta\xi(x, y) = 0, \quad (x, y) \in \Omega, \quad (2a)$$

$$\xi(x, y) = \cos\theta \quad \theta = \arg \gamma^{-1}(x, y) \quad (x, y) \in \partial\Omega, \quad (2b)$$

and

$$\Delta\eta(x, y) = 0, \quad (x, y) \in \Omega, \quad (3a)$$

$$\eta(x, y) = \sin\theta \quad \theta = \arg \gamma^{-1}(x, y) \quad (x, y) \in \partial\Omega, \quad (3b)$$

where, for $(x, y) \in \partial\Omega = \Gamma$, $\gamma^{-1}(x, y) = e^{i\theta} \in S^1$. In section 3, we will prove that $g|_{\Omega}$ is indeed a C^2 diffeomorphism. Therefore the inverse $f = g^{-1} : \overline{D} \rightarrow \overline{\Omega}$ exists and is differentiable on the interior. Transforming ξ, η to $\rho := \sqrt{\xi^2 + \eta^2}$ and $\theta := \arg(\xi + i\eta)$, where ρ, θ are polar coordinates on the unit disk, we obtain *boundary conforming coordinates* for Ω . In particular, $\rho \in [0, 1]$, with $\rho = 1$ on the boundary $\Gamma = \partial\Omega$, and $\theta \in [0, 2\pi)$. This situation is sketched in figure 2.

2.2. A simple example

We will now consider the simple example of an ellipse. The boundary Γ of the elliptical domain Ω is shown in figure 3. A parametrization of the boundary is given by

$$x = a \cos\theta, \quad (4)$$

$$y = b \sin\theta, \quad (5)$$

where a, b are the semi-major and semi-minor axes respectively and $\theta \in [0, 2\pi)$ is the periodic curve parameter. The boundary parametrization $\gamma : S^1 \rightarrow \mathbb{R}^2$ is then defined as

$$\gamma(\xi + i\eta) = \begin{pmatrix} a \cos\theta \\ b \sin\theta \end{pmatrix} = \begin{pmatrix} a\xi \\ b\eta \end{pmatrix}, \quad \xi + i\eta = e^{i\theta} \in S^1. \quad (6)$$

The solutions of (2a)-(3b) are

$$\xi(x, y) = \frac{x}{a}, \quad (x, y) \in \overline{\Omega} \quad (7)$$

$$\eta(x, y) = \frac{y}{b}, \quad (x, y) \in \overline{\Omega}. \quad (8)$$

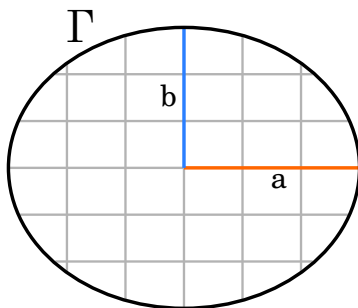


Figure 3. Sketch of an elliptical domain with boundary Γ in black, semi-major axis a in orange, semi-minor axis b in blue and equidistant contours of ξ and η in grey.

Therefore the harmonic map g is given by

$$g(x, y) = \frac{x}{a} + i\frac{y}{b}, \quad (x, y) \in \overline{\Omega}. \quad (9)$$

To check whether the boundary parametrization is preserved in the harmonic map, we can compute the composition $g \circ \gamma$ for all $\xi + i\eta \in S^1$:

$$\begin{aligned} g \circ \gamma(\xi + i\eta) &= g(\gamma(\xi + i\eta)) \\ &= g(a\xi, b\eta) \\ &= \frac{a\xi}{a} + i\frac{b\eta}{b} = \xi + i\eta, \end{aligned}$$

which is equal to the identity map, i.e. $g \circ \gamma = \text{Id}$.

The target mapping $f : \overline{D} \rightarrow \overline{\Omega}$ is the inverse of g , which evaluates to

$$f(\xi + i\eta) = \begin{pmatrix} a\xi \\ b\eta \end{pmatrix}, \quad \xi + i\eta \in \overline{D}, \quad (10)$$

$$f(\rho e^{i\theta}) = \begin{pmatrix} a\rho \cos \theta \\ b\rho \sin \theta \end{pmatrix}, \quad \rho e^{i\theta} \in \overline{D}. \quad (11)$$

The similarity of (6) and (10), i.e. that they only differ in the domain of definition, is specific to this example. In general, f and γ have to agree only on the boundary, i.e.

$$f(e^{i\theta}) = \gamma(e^{i\theta}), \quad \theta \in [0, 2\pi). \quad (12)$$

It is worth noting that this mapping is not conformal, but instead it gives the intuitive linear transformation of the unit disk to the ellipse, i.e. contours of constant ρ are ellipses with the same aspect ratio as the boundary.

2.3. Implementation

In general it is not possible to find analytic expressions for g . To obtain the harmonic map $g : \overline{\Omega} \rightarrow \overline{D}$, we solve the two Laplace-Dirichlet problems (2a)-(3b) using a boundary integral method [14]. We explicitly choose a boundary integral method to avoid discretizing the Laplace problem in Ω . Instead, the evaluation of the map g at arbitrary points in Ω reduces to a boundary integral over the density of the corresponding double layer potential [14, eq. 6.19]. This density can be interpreted as

dipole charges distributed on the boundary $\partial\Omega$, equivalent to the boundary conditions (2b) and (3b). For evaluations near the boundary, a correction is needed to account for the singularity of the Green's function [15, 16]. To obtain a discretized diffeomorphism $f_h \approx f = g^{-1} : \bar{D} \rightarrow \bar{\Omega}$, $\xi + i\eta \mapsto (x, y)$ we use the following algorithm:

- (i) Solve for the density of the double layer potential corresponding to the Dirichlet-Laplace problems (2a)-(3b). This now allows evaluation of $g(x, y) = \xi(x, y) + i\eta(x, y)$ at any point inside the domain, using a boundary integral.
- (ii) Choose a Zernike basis [17–19] (see Appendix B) with maximum polynomial degree M and determine the interpolation or integration points ξ_ℓ, η_ℓ , e.g. based on a concentric sampling pattern [20].
- (iii) Find $(x_\ell, y_\ell) \in \Omega$, such that $g(x_\ell, y_\ell) = \xi_\ell + i\eta_\ell$ with the Newton-Raphson method.
- (iv) Solve for the coefficients of the Zernike polynomials for the map f_h using the pointwise solution $\xi_\ell + i\eta_\ell \mapsto (x_\ell, y_\ell)$ found in step (iii)
- (v) Check the Jacobian determinant $\det f_h$ and refine the degree M if necessary, e.g. if $\det f_h(\xi + i\eta) < 0$ for any $\xi + i\eta \in D$ or $\min \det f_h \ll \min \det g^{-1}$, where $\det f_h$ and $\det g$ are the Jacobian determinants of f_h and g respectively. For the examples in section 4 we evaluate the Jacobian determinant of g pointwise on a regular grid in Ω and the Jacobian determinant of g^{-1} or f_h on a polar grid in D .

The proposed method is implemented in the `map2disc` † python package. To solve the Laplace problems for ξ and η , we use a fast and accurate boundary integral method, as implemented in the `pyBIE2D` python package [16].

3. Existence and regularity of the constructed mapping

In this section, we present the proof for the existence, regularity and invertibility of g .

Theorem 1. *Let $\Omega \subset \mathbb{R}^2$ be a simply connected domain bounded by a Jordan curve $\Gamma = \partial\Omega$ with C^2 parametrization $\gamma : S^1 \rightarrow \mathbb{R}^2$, with γ invertible on its image $\gamma(S^1) = \Gamma$. Then:*

(i) *There exists a unique map $g : \bar{\Omega} \rightarrow \bar{D}$ in $C(\bar{\Omega}) \cap C^2(\Omega)$ such that*

- $g \circ \gamma = \text{Id}$,
- g is a harmonic function in Ω ,

(ii) *The restriction $g|_\Omega$ is a C^2 diffeomorphism.*

Remark. *This theorem differs from the Riemann Mapping Theorem in that the map g is not necessarily a conformal map, which can be beneficial for discretization. However, if γ is identical to the boundary parametrization of a conformal map, then g is a conformal map. Note also that this theorem is similar to the Radó-Kneser-Choquet Theorem [21] and its generalization [22], but uses a harmonic map from a simply connected domain to the unit disk and not the reverse.*

† Available from the authors upon request.

Proof. Let $\xi, \eta \in C(\overline{\Omega}) \cap C^2(\Omega)$ be the solutions to the Dirichlet-Laplace problems (2a)-(3b). From [23, Corollary 11.13], it follows that the two Dirichlet problems are solvable, i.e., that ξ, η exist and are unique. Furthermore from [23, Theorem 1.28] it follows that ξ, η are real analytic in Ω .

Then by construction, g as defined in (1), is a complex-valued harmonic function in Ω and $g \circ \gamma = \text{Id}$, since, for any $z \in S^1$, $\theta := \arg z$,

$$\begin{aligned} g \circ \gamma(z) &= \xi \circ \gamma(z) + i\eta \circ \gamma(z) \\ &= \cos \theta + i \sin \theta \\ &= e^{i\theta} = z, \end{aligned}$$

given the boundary conditions (2b) and (3b).

By the inverse function theorem, a sufficient condition for $g|_{\Omega}$ to be a diffeomorphism is that the Jacobian matrix of g is invertible, which is the case if $\nabla \xi$ and $\nabla \eta$ are linearly independent.

Let $u \in C(\overline{\Omega}) \cap C^2(\Omega)$ be any normalized linear combination of ξ and η , i.e.

$$u := \frac{\alpha \xi + \beta \eta}{\sqrt{\alpha^2 + \beta^2}} \quad (\alpha, \beta) \in \mathbb{R}^2 \setminus \{(0, 0)\}, \quad (13)$$

where α, β are arbitrary but fixed. This is equivalent to

$$u := \xi \cos \phi + \eta \sin \phi \quad \phi \in [0, 2\pi), \quad (14)$$

with arbitrary but fixed ϕ , by defining $\phi := \arg(\alpha + i\beta)$.

Then u is a solution of the Dirichlet-Laplace problem

$$\Delta u(x, y) = 0 \quad (x, y) \in \Omega, \quad (15)$$

$$u(x, y) = \cos(\theta - \phi) \quad \theta = \arg \gamma^{-1}(x, y) \quad (x, y) \in \partial\Omega. \quad (16)$$

From [24, Theorem 1.1], it follows that the critical points of u in the interior of Ω are finite in number $K \in \mathbb{N}_0$, and denoting by m_1, \dots, m_K their multiplicities, we have:

$$\sum_{k=1}^K m_k \leq N - 1, \quad (17)$$

where N is the number of relative maxima of $u|_{\Gamma}$. For the case of (16), we check that $N = 1$ and thus $\sum_k m_k = 0$. Therefore any linear combination of ξ and η has no critical point in Ω , which implies that $\nabla \xi$ and $\nabla \eta$ are linearly independent. By the inverse function theorem, $g|_{\Omega}$ is then a C^2 diffeomorphism from Ω to D . \square

4. Numerical experiments

In order to assess the quality of a mapping $f : \overline{D} \rightarrow \overline{\Omega}$, we introduce a *normalized Jacobian determinant* within each cross-section

$$\mathcal{J}_n := \frac{\det f}{\max[\det f]} \leq 1, \quad (18)$$

which will also be used for visualization. The Jacobian determinant of the mapping $f : \bar{D} \rightarrow \bar{\Omega}$, $\xi + i\eta \mapsto (x, y)$ and its inverse $g := f^{-1}$ are defined as

$$\det f := \frac{\partial x}{\partial \xi} \frac{\partial y}{\partial \eta} - \frac{\partial x}{\partial \eta} \frac{\partial y}{\partial \xi}, \quad \det g := \frac{\partial \xi}{\partial x} \frac{\partial \eta}{\partial y} - \frac{\partial \xi}{\partial y} \frac{\partial \eta}{\partial x} = (\det f)^{-1}. \quad (19)$$

In practice, it is common to define the mapping using the polar coordinates ρ, θ for the unit disk. Then the Jacobian determinant of the boundary conforming mapping $h : (\rho, \theta) \mapsto (x, y) = f(\rho e^{i\theta})$ is related to $\det f$ by

$$\det h := \frac{\partial x}{\partial \rho} \frac{\partial y}{\partial \theta} - \frac{\partial x}{\partial \theta} \frac{\partial y}{\partial \rho} = \rho \det f. \quad (20)$$

The mapping f is invertible (and orientation preserving) if $\det f > 0$, thus $\mathcal{J}_n > 0$. In some regards, the “best” mapping has a constant Jacobian determinant, i.e. $\mathcal{J}_n = 1$ in the whole domain. This is motivated by affine maps of the unit disk, which have a constant Jacobian matrix and, thereby, a constant Jacobian determinant. In particular, a large ratio between the maximum and minimum Jacobian determinant, and therefore a small $\min \mathcal{J}_n$, often leads to problems with numerical methods without mesh refinement. On the other hand, this metric alone is not ideal as a certain “straightness” of the coordinate contours is desired [7].

4.1. Optimized stellarator

One example configuration where simple radial blending (see Appendix A) is not sufficient is an optimized two-field-period quasi-helically symmetric stellarator configuration found using the near-axis expansion method [5], provided as the 2022 QH nfp2 configuration of the pyQSC [25] library. As such, boundaries of this or similar configurations cannot be used with the default initialization method of VMEC and GVEC. Figure 4 shows coordinate contours for the boundary conforming coordinates ρ and θ on the $\phi = \pi/8$ cross-section for different initialization methods, with normalized Jacobian \mathcal{J}_n shown in color.

For radial blending, overlapping coordinate contours are clearly visible, and the Jacobian determinant assumes negative values in the regions of overlapping contours. Both the minimization of the squared Jacobian determinant [7] and the proposed method show no such overlapping contours, and the Jacobian determinant is positive everywhere. Coincidentally the central axis of both methods is close to the magnetic axis of the near-axis expansion, despite it not being specified in the construction. For the construction by minimizing $(\det g)^2$, it was necessary to choose a “small” value of the straightness weighting factor $\omega = 0.001$. This then produces a mapping with a more uniform distribution of \mathcal{J}_n than the mapping constructed with two harmonic functions, but the coordinate contours are less smooth.

4.2. Illustrative example and convergence analysis

To investigate the accuracy and convergence of the proposed method, we consider a conformal map $f_c : \bar{D} \rightarrow \bar{\Omega}$ of a sheared ellipse. The map $f_c = f_2 \circ f_1$ is shown in

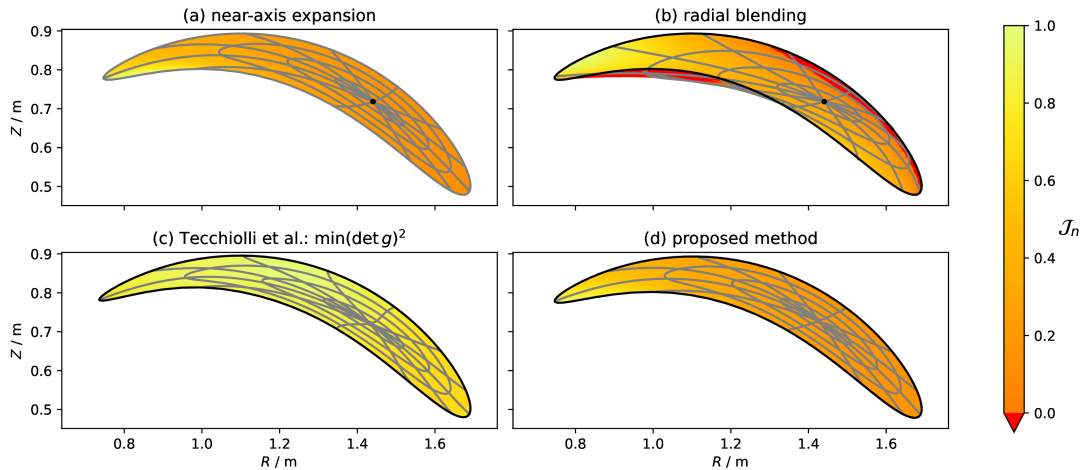


Figure 4. The $\phi = \pi/8$ poloidal cross-section of the optimized two-field-period quasi-helically symmetric stellarator generated from the near-axis method [5, 25]. The color shows the normalized Jacobian determinant (18), with yellow depicting regions with high \mathcal{J}_n , orange depicting regions of low \mathcal{J}_n , and red depicting invalid regions with negative \mathcal{J}_n . Contours of ρ and θ are grey, the prescribed boundary and/or axis is black. (a) is the near-axis solution. (b) is constructed using radial blending (see Appendix A). (c) is constructed by minimizing the squared Jacobian determinant [7] (with a straightness weighting coefficient of $\omega = 0.001$) and (d) is constructed using the proposed method.

figure 5 and is composed of the conformal map of the ellipse f_1 (see Appendix C) with semi-axes $a = 0.9$ and $b = 0.6$ and a polar map f_2 , representing the shear, defined as

$$f_2(z) := \exp \left[\frac{z}{2} \exp \left(\frac{i\pi}{12} \right) \right]. \quad (21)$$

As f_2 is a holomorphic function, it is a conformal map, and the composition f_c is also a conformal map. This particular map was chosen as it features a high complexity by requiring an infinite Fourier series to represent the boundary parametrization despite having a comparatively simple shape, and it shows less symmetry than the ellipse alone.

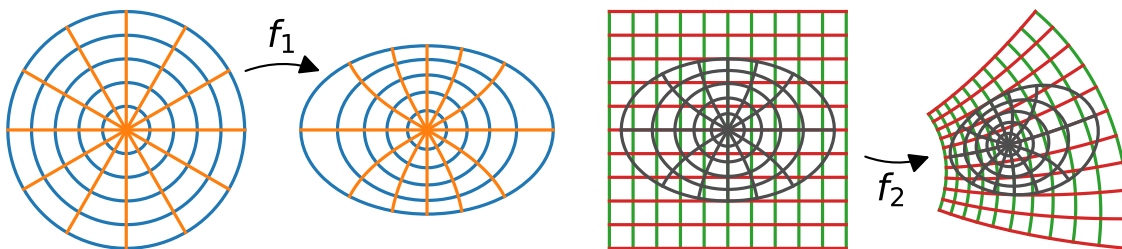


Figure 5. The two components of the conformal map $f_c = f_2 \circ f_1$. f_1 maps the unit disk to the ellipse and f_2 maps the plane to a polar domain. For f_1 the contours of ρ and θ are shown in blue and orange and for f_2 the contours of ξ and η are shown in green and red with the ρ and θ contours of the ellipse overlaid in grey.

The implementation of the analytic conformal map f_c and its inverse f_c^{-1} is accurate up to machine precision, with an error of

$$\max_{z \in \Omega} |f_c(f_c^{-1}(z)) - z| < 7.4 \cdot 10^{-16}.$$

Note that the errors were evaluated on a grid of 30076 points in Ω (selected from a bounding box of 200×200 points in \mathbb{R}^2). The harmonic map g , evaluated with the boundary integral method as implemented in pyBIE2D with 500 points on the boundary shows an error of

$$\max_{z \in \Omega} |f_c(g(z)) - z| < 2.87 \cdot 10^{-14}.$$

The negligible difference between g and f_c shows that with our implementation, the specification of a boundary parametrization of a conformal map reproduces this conformal map. The numerical inversion with Newton iterations (with the default tolerance of 10^{-8} in the $\xi + i\eta$ position) shows an only marginally higher error of

$$\max_{z \in \Omega} |g^{-1}(f_c^{-1}(z)) - z| < 2.89 \cdot 10^{-14}. \quad (22)$$

The error of the discrete approximation f_h depends strongly on the number of basis functions K and the maximum degree M , as shown in figure 6.

Figure 6 shows the conformal map f_c at the left and the maximum error of the discrete approximation $f_h \approx f_c$ by projection onto a Zernike basis (see Appendix B) with maximum degree M and corresponding number of basis functions K at the right. The projection is performed using Gaussian quadrature in ρ with $4(M+1)$ points and

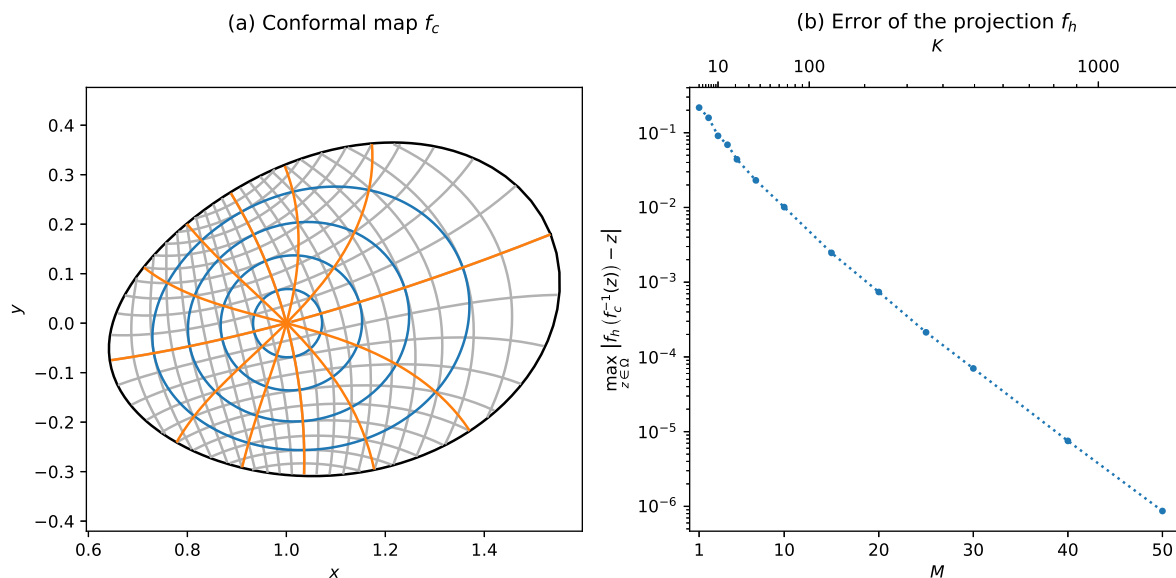


Figure 6. (a) The conformal map f_c with contours of ρ and θ in blue and orange respectively and contours of ξ and η in grey. (b) Maximum error of the discrete approximation $f_h \approx f_c$ by projection onto a Zernike basis with maximum degree M and corresponding number of basis functions K .

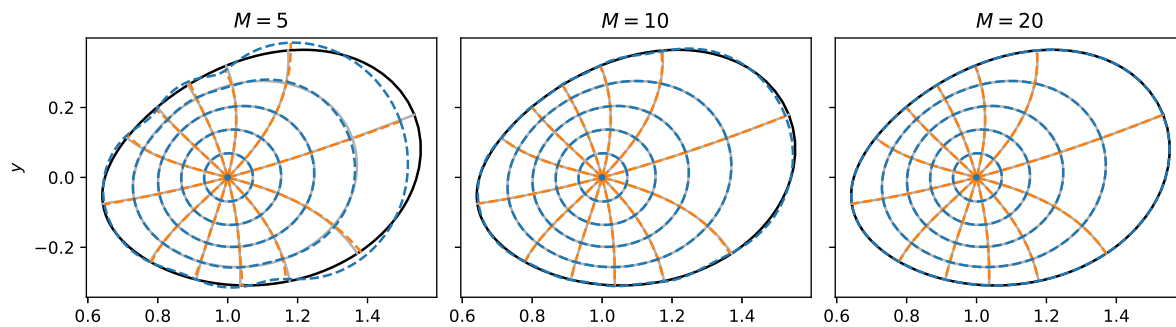


Figure 7. Discrete approximations $f_h \approx f_c$ of the conformal map of a sheared ellipse, constructed by projection onto a Zernike basis with different maximum degrees M . Contours of ρ and θ are blue and orange for f_h , respectively, and grey for f_c . The boundary of f_c is black.

the trapezoidal rule in θ with $4(2M + 1)$ points. In the semi-logarithmic plot, the error decreases in a manner characteristic of spectral convergence in M , but it only reaches values of 10^{-6} for $M = 50$, which already requires $K = 1326$ basis functions. This low accuracy is due to the high complexity of f_c and the resulting high number of Fourier modes required to accurately represent the boundary parametrization. Figure 7 shows three different discrete approximations of this mapping, visually displaying the convergence seen on the right of figure 6. In particular, for low numbers of M , the mapping seems to be accurate near the axis but cannot accurately represent the boundary of the domain. This is consistent with the fact that the boundary requires many Fourier modes to be well-representable and that conformal maps tend to become circular around the axis.

4.3. More examples

One of the key benefits of the proposed method is that the construction is provably invertible for arbitrarily shaped domains. In figure 8, we show the contour lines of ρ and the normalized Jacobian determinant \mathcal{J}_n for the discrete approximations f_h of the mapping g^{-1} for three different, strongly shaped domains. The mappings are discretized by interpolation with a Zernike basis of maximum degree $M = 15$. Even though the Jacobian determinant and, thereby, the density of contour lines can vary strongly within the domain, \mathcal{J}_n is always positive, and the mapping is thus invertible. Note that for the “star” domain, it is challenging to find a numerical conformal map [26].

The mappings for the “boomerang” and “star” domains represent the boundary of the domain with machine precision, i.e.

$$\varepsilon := \frac{1}{d} \max_{z \in \partial\Omega} |f_h(\gamma^{-1}(z)) - z| < 4 \cdot 10^{-15},$$

relative to the maximum extent d of the domain Ω . The mapping for the “worm” domain, for which the boundary has been specified using B-splines, has a maximum

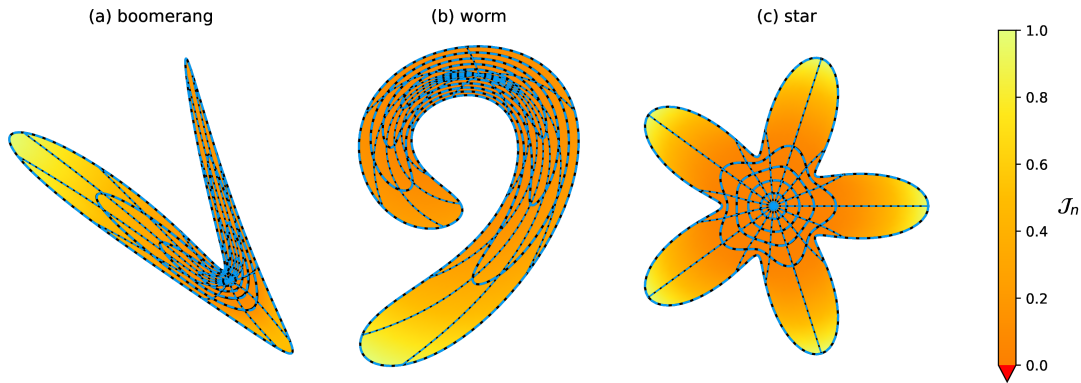


Figure 8. Boundary conforming mappings for three strongly shaped domains. Contour lines of ρ and θ for the harmonic mapping g are in black, and for the corresponding discrete mapping f_h in blue, constructed by interpolation with a Zernike basis of maximum degree $M = 15$. The domain is colored with the normalized Jacobian determinant (18) of the discrete mapping f_h .

error of the boundary representation of

$$\varepsilon < 4 \cdot 10^{-5}.$$

This error decreases with increasing maximum degree M , similar to the convergence of the conformal map in figure 6.

5. Conclusion

The presented novel method allows the construction of a mapping from an arbitrary, simply connected two-dimensional domain, bounded by a Jordan curve to the unit disk, by solving two Dirichlet-Laplace problems using a boundary integral method. Our method therefore separates the construction of a discrete mapping into two parts: In the first step, the harmonic mapping is generated, which can be evaluated at arbitrary points using the boundary integral and is provably invertible. The second step is then the discrete approximation of the inverse of the harmonic map with a suitable method, e.g. by projection or interpolation of a Zernike polynomial basis. We have proven that the harmonic mapping is a diffeomorphism on the interior by leveraging known theorems about the properties of harmonic functions. Thus the mapping is invertible and can be used to define boundary conforming coordinates. This method does not require knowledge of the axis for the construction of the mapping. The parameterization of the boundary and the resolution of the discrete mapping are the only free parameters in the proposed method. If the parametrization of the boundary is chosen to be the same as the one obtained by means of a conformal map, the construction will yield exactly this conformal map. However, we find the conformal map to be difficult to discretize using Zernike polynomials, as shown in figure 6. Nevertheless, the maximum error of the discretization decreases in a spectral manner, which implies that the Zernike basis

is in general well suited for the discretization of such mappings. This can also be seen in figure 8, which shows three examples of strongly shaped domains where a valid mapping is constructed and discretized successfully.

One of the motivations for this work was the initialization of 3D MHD equilibrium codes, which need to find torus-like coordinates, given a plasma boundary. For strongly shaped boundaries, e.g., as shown in figure 4, the simple radial blending of the boundary Fourier modes does not work. While the proposed method works with two-dimensional domains, it can be extended to toroidal domains by applying it on a series of poloidal cross-sections.

Moreover, the proposed method can also be applied in other fields where boundary conforming coordinates for toroidal or cylinder-like domains are required. The construction of a harmonic mapping and discretization using Zernike polynomials is implemented in the `map2disc` § python package for arbitrary, simply connected 2D domains. It is intended to be extended for 3D plasma boundaries with interfaces for the VMEC and GVEC 3D MHD equilibrium solvers.

Plasma boundaries for 3D MHD configurations are typically described using Fourier series. Therefore the discrete approximation of the constructed mapping can represent the prescribed boundary exactly, provided the maximum degree of Zernike polynomials is at least the maximum number of Fourier modes of the boundary. Approximation errors of the discrete mapping in the interior are not as important, as long as the mapping is invertible, particularly when this mapping is used as the initialization for an MHD equilibrium solver. Finally, some applications do not require a discrete approximation but just the evaluation of the mapping or its inverse on a number of points. In this case, the harmonic mapping can be evaluated directly with high accuracy, and a discretization of the mapping is not necessary.

Acknowledgments

The authors would like to thank our colleagues at the Numerical Methods in Plasma Physics division at IPP Garching for the insightful discussions, in particular Alexander Hoffmann, Martin Campos Pinto, and Eric Sonnendrücker, who helped us with the formulation of the proof.

We would also like to greatly thank David Stein from Flatiron Institute, New York, for providing the `pyBIE2D` python package [16], a fast, open-source python-based implementation of a 2D boundary integral solver, based on Alex Barnett's package `BIE2D` written for matlab [15]. The availability and simplicity of `pyBIE2D` made this project possible in the first place and allowed us to focus our implementation effort within the `map2disc` python package on the discrete approximations of the mapping.

We would also like to thank Stuart Hudson, Joaquim Loizu and the group around SPEC for drawing our attention to the problem of initialization in 3D MHD codes and for discussions on the topic.

§ Available from the authors upon request.

This work has been carried out within the framework of the EUROfusion Consortium, funded by the European Union via the Euratom Research and Training Programme (Grant Agreement No 101052200 — EUROfusion). Views and opinions expressed are however those of the author(s) only and do not necessarily reflect those of the European Union or the European Commission. Neither the European Union nor the European Commission can be held responsible for them.

Robert Köberl is supported by the Helmholtz Association under the joint research school “Munich School for Data Science - MUDES”.

Data availability statement

The data that support the findings of this study are openly available in Zenodo at <https://zenodo.org/records/13318488>.

Appendix A. Radial blending technique

A simple technique to construct a mapping $f : \bar{D} \rightarrow \mathbb{R}^2$ from the unit disk to a domain bounded by a simple closed curve Γ is radial blending of the Fourier components of the boundary [6]. Let the boundary parametrization $\gamma : S^1 \rightarrow \mathbb{R}^2$, with $\gamma(S^1) = \Gamma$, be given by the Fourier series

$$\gamma(e^{i\theta}) = \sum_{m=0}^M \gamma_m^c \cos(m\theta) + \gamma_m^s \sin(m\theta), \quad (\text{A.1})$$

where $\gamma_m^c, \gamma_m^s \in \mathbb{R}^2$ are the Fourier coefficients and let $a \in \mathbb{R}^2$ be the position of the axis, i.e. $f(0) := a$. Then the radial blending technique constructs the mapping using polar coordinates as

$$f(\rho e^{i\theta}) = \sum_{m=0}^M f_m^c(\rho) \cos(m\theta) + f_m^s(\rho) \sin(m\theta), \quad (\text{A.2})$$

where the Fourier coefficients are defined as

$$f_0^c(\rho) = a + (\gamma_0^c - a) \rho^2 \quad (\text{A.3})$$

$$f_0^s(\rho) = 0 \quad (\text{A.4})$$

$$f_m^{c,s}(\rho) = \gamma_m^{c,s} \rho^m \quad 0 < m \leq M. \quad (\text{A.5})$$

This mapping fulfills the boundary conditions $f(e^{i\theta}) = \gamma(e^{i\theta})$ and $f(0) = a$, but is not necessarily invertible and can map to points outside of the boundary Γ .

Appendix B. Zernike polynomials

Zernike polynomials [17–19] are a set of orthogonal polynomials on the unit disk. They are convenient for the discretization of smooth functions on the unit disk, as they are

polynomials in the Cartesian coordinates ξ, η , but also have a simple representation in polar coordinates ρ, θ . They are defined as

$$Z_l^m(\rho, \theta) = \begin{cases} R_l^m(\rho) \cos(m\theta) & m \geq 0, \\ R_l^m(\rho) \sin(-m\theta) & m < 0, \end{cases} \quad m = -l, -l+2, \dots, l, \quad (\text{B.1})$$

where the radial polynomials R_l^m are defined as

$$R_l^m(\rho) = (-1)^{(l-m)/2} \rho^m P_{(l-m)/2}^{m,0}(1-2\rho^2), \quad (\text{B.2})$$

with the Jacobi polynomials $P_{(l-m)/2}^{m,0}$.

In this work, a Zernike base of maximum degree M contains the polynomials Z_l^m with $l = 0, 1, \dots, M$, and $m = -l, -l+2, \dots, l$ for each l . It therefore contains $K = (M+1)(M+2)/2$ basis functions. From the definition above, it is clear that the maximum degree M has a direct relation to the maximum mode number of the Fourier series in the angle θ .

In this work, the interpolation points for the Zernike polynomials are chosen based on a concentric sampling pattern [20]. They are placed on $\lfloor \frac{M}{2} \rfloor + 1$ rings, whose position is determined by Chebyshev-Lobatto points of degree M , defined as

$$\rho_i = \cos\left(\frac{i\pi}{M}\right), \quad 0 \leq i \leq \left\lfloor \frac{M}{2} \right\rfloor. \quad (\text{B.3})$$

On each ring, $2M+1-4i$ points are placed equidistantly:

$$\theta_{ij} = \frac{2\pi j}{2M+1-4i}, \quad 0 \leq j \leq 2M-4i, \quad 0 \leq i \leq \left\lfloor \frac{M}{2} \right\rfloor. \quad (\text{B.4})$$

Appendix C. Conformal map of an ellipse

In this section, an analytical expression of the conformal map from the unit disk to the ellipse, as depicted in the left part of figure 5, as well as the expression of its inverse, are presented. They are found in [27–29].

Given an ellipse in the complex plane, centered at the origin with semi-major axis a and semi-minor axis b , the analytical expression of the conformal map from the unit disk in the complex plane $|\xi + i\eta| \leq 1$ to the ellipse reads as

$$f_{\text{ell}}(\xi + i\eta) = c \sin\left(\frac{\pi}{2} \frac{\text{F}\left(\arcsin\left(\frac{(\xi + i\eta)/\sqrt{k}, k^2\right), k^2\right)}{\text{K}(k^2)}\right), \quad (\text{C.1})$$

with the linear eccentricity $c = \sqrt{a^2 - b^2}$, the Legendre incomplete elliptic integral of the first kind $\text{F}(\phi, m)$, the complete elliptic integral $\text{K}(m) = \text{F}(\pi/2, m)$, the elliptic parameter $m = k^2$, using the elliptic modulus computed as $k = (\vartheta_2(q)/\vartheta_3(q))^2$ from the Jacobi theta functions and the elliptic nome $q = (a-b)^2/(a+b)^2$. The x, y coordinates of the ellipse in \mathbb{R}^2 are simply computed from the real and imaginary part of f_{ell} .

The inverse of the map $g_{\text{ell}} = (f_{\text{ell}})^{-1}$ is expressed analytically as

$$g_{\text{ell}}(x, y) = \sqrt{k} \text{sn}\left(\frac{2}{\pi} \text{K}(k^2) \arcsin\left(\frac{x + iy}{c}\right), k^2\right) \quad (\text{C.2})$$

where $\operatorname{sn}(u, m)$ is the Jacobi elliptic function, and $g_{\text{ell}} = \xi + i\eta$ is the position on the unit disk. An implementation of these functions using the `mpmath` [30] python package is included in the `map2disc` package.

References

- [1] Hirshman S P and Whitson J C 1983 *Physics of Fluids* **26** 3553–3568 ISSN 0031-9171
- [2] Hindenlang F 2019 A newly developed 3d ideal mhd galerkin variational equilibrium code
- [3] Garren D A and Boozer A H 1991 *Physics of Fluids B: Plasma Physics* **3** 2805–2821 ISSN 0899-8221
- [4] Garren D A and Boozer A H 1991 *Physics of Fluids B: Plasma Physics* **3** 2822–2834 ISSN 0899-8221
- [5] Landreman M 2022 *Journal of Plasma Physics* **88** 905880616 ISSN 0022-3778, 1469-7807
- [6] Qu Z S, Pfefferlé D, Hudson S R, Baillo d A, Kumar A, Dewar R L and Hole M J 2020 *Plasma Physics and Controlled Fusion* **62** 124004 ISSN 0741-3335
- [7] Tecchiolli Z, Hudson S, Loizu J, Köberl R, Hindenlang F and De Lucca B 2024 Constructing nested coordinates inside strongly shaped toroids using an action principle (*Preprint* 2405.08173)
- [8] Thompson J F 1982 *Applied Mathematics and Computation* **10-11** 79–105 ISSN 0096-3003
- [9] Winslow A M 1966 *Journal of computational physics* **1** 149–172
- [10] Knupp P M 1992 *Journal of Computational Physics* **100** 409–418 ISSN 0021-9991
- [11] Charakhch'yan A and Ivanenko S 1997 *Journal of Computational Physics* **136** 385–398
- [12] Fortunato M and Persson P O 2016 *Journal of Computational Physics* **307** 1–14 ISSN 0021-9991
- [13] Duren P 2004 *Harmonic Mappings in the Plane* Cambridge Tracts in Mathematics (Cambridge: Cambridge University Press) ISBN 978-0-521-64121-0
- [14] Kress R 1999 *Linear Integral Equations (Applied Mathematical Sciences vol 82)* (New York, NY: Springer) ISBN 978-1-4612-6817-8 978-1-4612-0559-3
- [15] Barnett A, Wu B, Marple G, Trefethen N and Wang J 2021 BIE2D: MATLAB tools for boundary integral equations on curves in 2D
- [16] Stein D pyBIE2D: Python Tools for Boundary Integral Equations in 2D Flatiron Institute
- [17] Zernike F and Stratton F 1934 *Monthly Notices of the Royal Astronomical Society* **94** 377–384 ISSN 0035-8711
- [18] Boyd J P and Yu F 2011 *Journal of Computational Physics* **230** 1408–1438 ISSN 0021-9991
- [19] Dudd D W and Kolemen E 2020 *Physics of Plasmas* **27** 102513 ISSN 1070-664X
- [20] Ramos-López D, Sánchez-Granero M A, Fernández-Martínez M and Martínez-Finkelshtein A 2016 *Applied Mathematics and Computation* **274** 247–257 ISSN 0096-3003
- [21] Kneser H 1926 *Jahresbericht der Deutschen Mathematiker-Vereinigung* **35** 123–124
- [22] Alessandrini G and Nesi V 2009 *Annali della Scuola Normale Superiore di Pisa - Classe di Scienze* **8** 451–468
- [23] Axler S, Bourdon P and Ramey W 2001 *Harmonic Function Theory (Graduate Texts in Mathematics vol 137)* (New York, NY: Springer) ISBN 978-1-4419-2911-2 978-1-4757-8137-3
- [24] Alessandrini G 1987 *Annali della Scuola Normale Superiore di Pisa - Classe di Scienze* **14** 229–256 ISSN 2036-2145
- [25] Landreman M and Jorge R 2024 pyQSC: Python implementation of the Quasisymmetric Stellarator Construction method
- [26] Trefethen L N 2020 *Computational Methods and Function Theory* **20** 369–387 ISSN 2195-3724
- [27] Schwarz H A 1869 *Journal für die reine und angewandte Mathematik* **70** 105–120
- [28] Schwarz H A 1890 *Springer, Berlin* 102–107 (in italian)
- [29] Szegő G 1950 *The American Mathematical Monthly* **57** 474–478
- [30] The mpmath development team 2023 Mpmath: A Python library for arbitrary-precision floating-point arithmetic